Supplementary Information

for

Revealing the impact of the host-salt non-stoichiometry on the performance of perovskite solar cells

Amit Kumar,[a] Bhanu Pratap Dhamaniya,[ab] Shailendra Kumar Gupta,[ac] Priyanka Chhillar,[a] Kartiki Chandratre,[a] Sandeep Kumar Pathak,[a] Supravat Karak*[a]

a. Department of Energy Science and Engineering, Indian Institute of Technology Delhi, Hauz Khas New Delhi-110016, India

b. Present address: U.R.Rao Satellite Centre, Indian Space Research Organisation, Bengaluru 560017, Karnataka India

c. Present address: Amity School of Physical Sciences, Amity University Punjab, IT City, Sector 82A, Mohali, 140308, India

*Corresponding Author: supravat@dese.iitd.ac.in

Contents

A. Experimental Section

1. Materials

Tin (IV) chloride pentahydrate (98%), Tin (II) chloride dihydrate (99.999%), Urea (99.5%), Thioglycolic acid (99%), CsI (99.999%), N,N-Dimethylformamide (99.8%), Dimethyl sulfoxide (99.9%), Anisole (99.7%), Li-TFSI (99.95%) and 4-*tert*-Butylpyridine (98%) were purchased from Sigma Aldrich. 36.5 wt.% Hydrochloric acid (99.999%) from Alfa Aesar. Organic salts $CH(NH_2)_2I$ (>99.0%) and CH_3NH_3I (>99.0%) were obtained from Greatcell Solar. PbI_2 (99.99%) and CsCl (>99.0%) acquired from TCI. Spiro-OMeTAD (>99.5%) was purchased from Lumtec. All the salts and solvents were used without further purification.

2. Solar Cell Fabrication

Glass Substrate Preparation

Fluorine-doped tin oxide (FTO) glass substrates were etched with the help of zinc powder and 2M hydrochloric acid to make desired patterns (Pilkington TEC7, 2.2 mm thick with sheet resistance 7-8 ohm/sq.). The substrates were then rinsed in deionized water (DI water), scrubbed with 1% Hellmanex (by volume in DI water) solution. Followed by sonication in Acetone, DI water and isopropanol for 5 minutes each and dried with the help of nitrogen gun. Finally, the substrates were cured in UV-Ozone chamber for 15 minutes.

Tin Oxide Electron Transport Layer Deposition

Tin oxide layers were grown over FTO with the help of chemical bath deposition method. 0.05M Tin(IV) Chloride Pentahydrate was prepared in isopropanol by shaking for 30 minutes. The solution was then spin-coated over cured substrates at 3000 rpm for 30 seconds (acceleration 200) and annealed at 180°C for an hour. Chemical bath comprises of 0.250 g urea, 50 µl thioglycolic acid, 2.5 ml hydrochloric acid and tin(II) chloride dihydrate at 0.012M. Substrates were placed in the chemical bath for 3 hours at 70°C in lab oven. Chemically cured substrates were then rinsed & sonicated in DI water for 2 minutes and finally annealed at 180°C for an hour.

Perovskite Precursor Preparation and Deposition

A 1.45M precursor solution was prepared with caesium chloride (12.20 mg), formamidine hydroiodide (236.88 mg) and lead (II) iodide (668.46 mg). Finally, methylamine hydriodide was

added into precursor with 0, 3, 5, 7, 9, 11, 15 and 20 mol%. All the precursor salts were dissolved in the anhydrous N,N-Dimethylformamide (DMF) and Dimethyl Sulfoxide (DMSO) at the fixed 4:1 vol/vol. Followed by the stirring over a hot plate at 70°C for half an hour. Perovskite thin-film deposition was carried in the dry box with controlled humidity at 10-20%. 70 µl of the precursor was spread over SnO_2 coated FTO substrate and spin at 6000 rpm for 35 seconds (acceleration 2000). 100 µl of anhydrous-Anisole was drenched 10 seconds prior to end the spin program for solvent quenching. The substrates were then immediately transfer over a hot plate at 150°C and annealed for 30 minutes. Then a thin PEAI (5 mM in IPA) deposited on top of perovskite films at 5000 rpm for 30 seconds (acceleration 3000) without annealing. We have fabricated 8 devices for each MAI variation.

Spiro-OMeTAD Hole Transport Layer Deposition

The Spiro-OMeTAD was immediately deposited over perovskite thin-film once the substrates were cooled down, at 2500 rpm for 25 seconds (acceleration 1000). Solution was prepared by dissolving 85 mg/ml Spiro-OMeTAD in chlorobenzene and was then doped with 20 µl bis(trifluoromethane)-sulfonimide lithium (Li-TFSI 500 mg/ml in acetonitrile) & 33 µl 4-tert butylpyridine (tBP). As deposited thin-film, devices were left in the desiccator (<5%RH) overnight for spiro-OMeTAD oxidation.

Au Counter-Electrode Deposition

The desired area of the device was scratched with the help of razor blade for FTO side contact and then 80 nm thick gold layer was thermally deposited under the vacuum of 6 x 10^{-6} torr.

3. Characterization

The J-V curves were measured using AM1.5 sunlight at 100 mW cm^{-2} (Keithley source meter 2400 series, USA) irradiance produced by an Abet class AAB 2000 solar simulator. The intensity was calibrated with an NREL calibrated KG5 filtered reference Si cell. J-V scan ranges from -0.049V to +1.2V with a scan range of 30 mV ms^{-1} and 5 seconds initial illumination stabilization time. The device active area was 0.25 cm^{-2} and 1 cm^2 using a metal aperture mask. The SSPL measurements were performed with Shimadzu RF-6000 series spectrofluorometer and the

perovskite films were prepared over cleaned glass substrate by spin-coating. The PLQE measurement were performed by exciting perovskite thin-films using 532 nm laser source, which is calibrated to measure at 1 sun. TRPL Data was recorded using a time correlated single photon counting (TCSPC) setup (FluoTime 300 PicoQuant GmbH). The samples were prepared over cleaned glass substrate and photoexcited using a 635 nm laser head (LDP-P-C-510, PicoQuant GmbH) of frequency 1MHz and a fluence of 2.41 nJ cm^{-2} per pulse. Absorbance spectrum was measured with the help of a Varian Cary 1050UV-VIS spectrophotometer (Agilent Technologies). The measurements were performed using Hitachi (Model S-4800) to acquire SEM images and perovskite films were deposited over FTO/c-SnO_2 layer. Electron beam was accelerated at 5-10.00 KV by the instrument. The XRD measurements were performed over perovskite deposited FTO/c-SnO_2 substrate using PANalytical X'Pert Pro XRD diffractometer with CuKα radiation source (λ 1.54 Å).

B. Supporting Notes

Note 1 – Photoluminescence quantum efficiency (PLQE) relating $V_{oc,non\text{-}rad}$

The theoretical limit of V_{oc} as per the principle of detailed balance, with considering the case where the radiative recombination of electron-hole pair is only channel for a single-junction cell. This is an assumption considered for the maximum conversion efficiency of a solar cell as of Shockley-Queisser limit[1]. Here, we note the V_{oc} for cells (practical) in terms of quantum efficiencies where the presence of non-radiative recombination (NRR) processes concludes internal quantum efficiencies smaller than unity[2]. The general form of V_{oc} expressed as[3,4]:

$$V_{oc} = \frac{K_B T}{q} ln\left(\frac{J_{SC}}{J_o}\right) \quad \text{(S1)}$$

The dark recombination current (J_o) and quantum efficiency of luminescence (η_{EL})[4]:

$$J_0 = \frac{q}{\eta_{EL}} \int EQE_{PV}(E)\Phi_{BB}(E)dE \quad \text{(S2)}$$

The photocurrent expressed as by multiplying EQE_{PV} with solar photon flux $\Phi_{AM1.5G}$ as a function of energy[3]:

$$J_{SC} = q \int EQE_{PV}(E)\Phi_{AM1.5G}(E)dE \quad \text{(S3)}$$

We note that for the ideal case when there is no non-radiative recombination i.e., η_{EL}=1 (equation 2), solar cell are approaching towards max SQ-limit. It is possible when measured V_{oc} is equal to radiative limit (i.e., Voc = $V_{oc,\,rad}$, i.e., non-radiative recombination current (J_{ne}) is ~0 at a given voltage (V)[5]. The $V_{oc,\,rad}$ is the radiative limit of open circuit voltage. From above two current expressions, both components are mostly determined by EQE_{PV}. The equation (S2 and S3) interprets to maximize the V_{oc} by when η_{EL} unity, it is V_{oc} radiative limit. And this is the case, when EQE_{LED} is unity. A solar cell, considering only radiative recombination, should act as LED with a maximum luminescence efficiency. We note that $V_{oc,\,rad}$ is still far from $V_{oc,\,SQ}$, as it requires step absorbance. Mathematically, both the terms related as[5]:

$$V_{oc,rad} = V_{oc,SQ} - KTln\left(\frac{J_{sc,SQ}}{J_{sc}}\right) - KTln\left(\frac{J_{o,rad}}{J_{o,SQ}}\right) \quad \text{(S4)}$$

Thus, the open-circuit voltage at max-SQ estimated as: $qV_{oc,SQ} = 0.941E_{g,PV} - 0.171eV$ [6]. This is expressed in terms of quantum efficiencies with its value at unity and under unity values as more generalized approach. Considering non-radiative recombination losses only[5]:

$$V_{oc,non-rad} = \frac{K_B T}{q} ln\left(\frac{1}{\eta_{EL}}\right) \quad \text{(S5)}$$

Therefore, the equation (S5) shows that low values of η_{EL} owing to NRR channels ($J_o>0$) accompanied by SRH recombination will result in loss of V_{oc}, where, $\eta_{EL} = \gamma\, \Phi_{PL}\, \eta_{out}$, where χ is light-out coupling factor, γ is charge balance factor and $\Phi_{PL}\, or\, \varphi$ is quantum efficiency of luminescence. From equation S(1-5), the following expression can be obtained (as of reference Rau2007[5]), $V_{oc} = V_{oc,\,rad} - V_{oc,non-rad}$. Mathematically, the relationship between V_{oc} and recombination can be described as:

$$V_{oc} = \frac{K_B T}{q} ln\left(\frac{\int_0^\infty EQE_{PV}(E)\Phi_{AM1.5G}(E)dE}{\int_0^\infty EQE_{PV}(E)\Phi_{BB}(E)dE}\right) - \frac{K_B T}{q} ln\left(\frac{1}{\eta_{EL}}\right) \quad \text{(S6)}$$

The term η_{EL} i.e., luminescence quantum efficiency is result in loss of V_{oc} if being less than 1, as discussed above. However, the logarithmic relation account for small reduction or improvement.

Note 2 – Photoluminescence decay fitting

Time-resolved photoluminescence spectroscopy (TRPL) is a powerful technique in understanding recombination kinetics of excited charge-carrier by fast (order of picoseconds) decay, called fluorescence. The lifetime is an intrinsic property of semiconductor material. In a semiconductor material common recombination mechanism are thought to be monomolecular (band-to-band) and bimolecular (trap-mediated recombination). The recombination rate constant is an important parameter and a strong function of initial carrier concentration, which is strongly influenced by the intensity and excitation repetition rate. Fitting of the resultant profile based on monomolecular or bimolecular trapping or bimolecular trapping detrapping model bring further

complexity (for the brief please see reference [7,8]). Therefore, for the simplicity of measurement, here, we consider single exponential fitting model, which we discuss below.

Fitting Model–

Here, the TRPL spectra of perovskite compositions with different MAI concentration using time-corelated single-photon counting (TCSPC). The PL decay was recorded for respective samples at a low 2.41 nJ cm^{-2} (pulsed 1 MHz repetition rate) owing to minimize carrier annihilation and non-geminate recombination with a 635nm laser source and characterized by stretched dynamics i.e., by fitting single exponential decay curve as depict by equation (S7).

$$I(t) = I_o e^{-(\frac{t}{\tau_c})^{\beta}} \quad \text{(S7)}$$

where $I(t)$ is the time dependent PL intensity, I_o is initial PL intensity, t is time, τ_c is characteristic lifetime and β is distribution coefficient.

Note 3 - Quasi-fermi level splitting (QFLS) calculation

The quasi-fermi level splitting (QFLS) is defining the maximum achievable open-circuit voltage (E_{FC} and E_{FV}, fermi energy corresponds to conduction band and valence band, respectively), representing the density of photogenerated free charge carriers, under equilibrium. We determined QFLS by following expression[9,10]:

$$QFLS = K_B T ln\left(PLQY \frac{J_G}{J_{O,rad}}\right) \quad \text{(S8)}$$

where K_B stands for the Boltzmann constant, T absolute temperature and PLQY photoluminescence. The terms J_G is the generation current and $J_{o,rad}$ is the dark radiative recombination current, both which are expressed by equation S2 and S3. Under the SQ assumptions, that PLQY is unity, where there are no non-radiative recombination losses will occur, we obtain the expression for 'QFLS under the radiative limit':

$$QFLS_{rad} = K_B T ln\left(\frac{J_G}{J_{O,rad}}\right) \quad \text{(S9)}$$

Net QFLS then represented as:

$$QFLS = QFLS_{rad} + K_B T ln(PLQY) \quad \text{(S10)}$$

The expression denoted in second term is representing the losses associated with non-radiative recombination. Therefore, in figure 4(e), we show the contribution of NRR loses in context of V_{oc} deviation from $QFLS_{rad}$.

C. Supporting figures

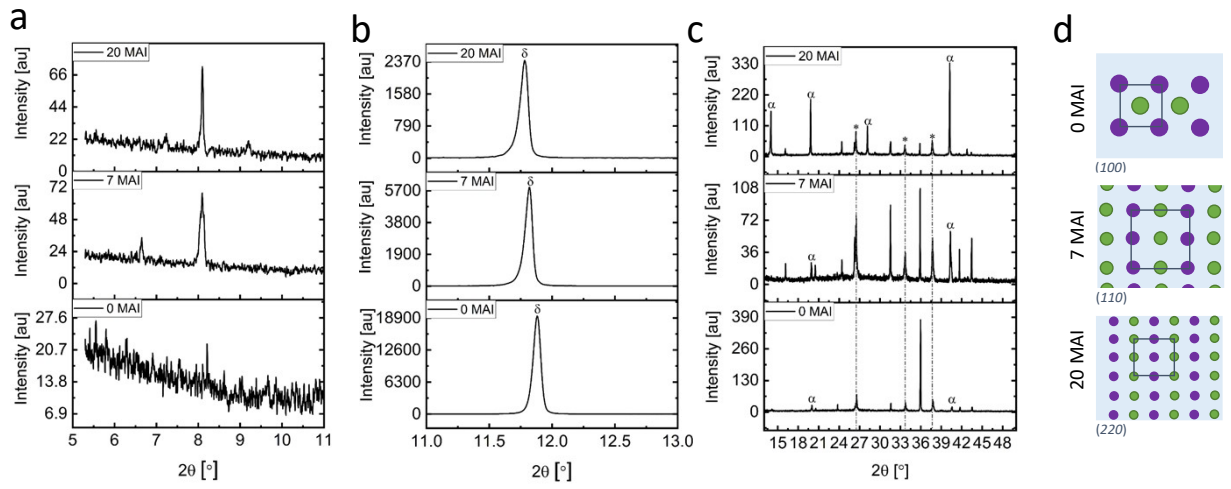

Fig. S1 The X-ray diffraction spectra of unannealed perovskite compositions with varying MAI concentrations deposited over FTO substrates. The XRD peaks corresponding to cubic phase $FAPbI_3$ (α symbol), PbI_2 (delta symbol), and FTO (asterisk symbol) are marked. The 2 theta compares in (a) 5-11˚, (b) 11-13˚, and (c) 13-50˚.

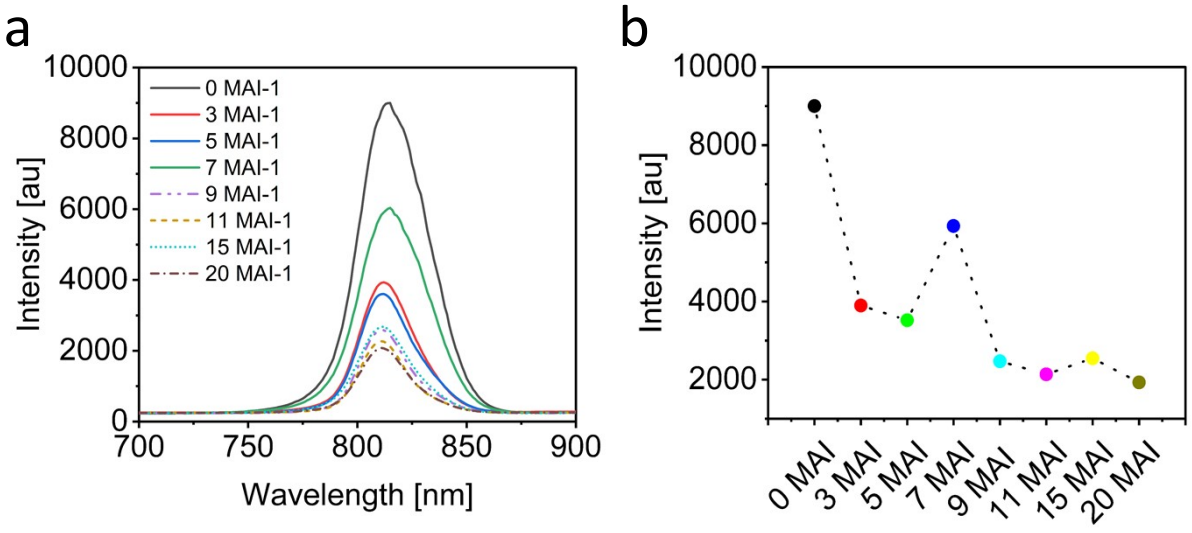

Fig. S2 Steady state photoluminescence (SSPL) spectra recorded for perovskite thin films as a function of MAI content when exciting by 520nm wavelength is compared in (a) and (b).

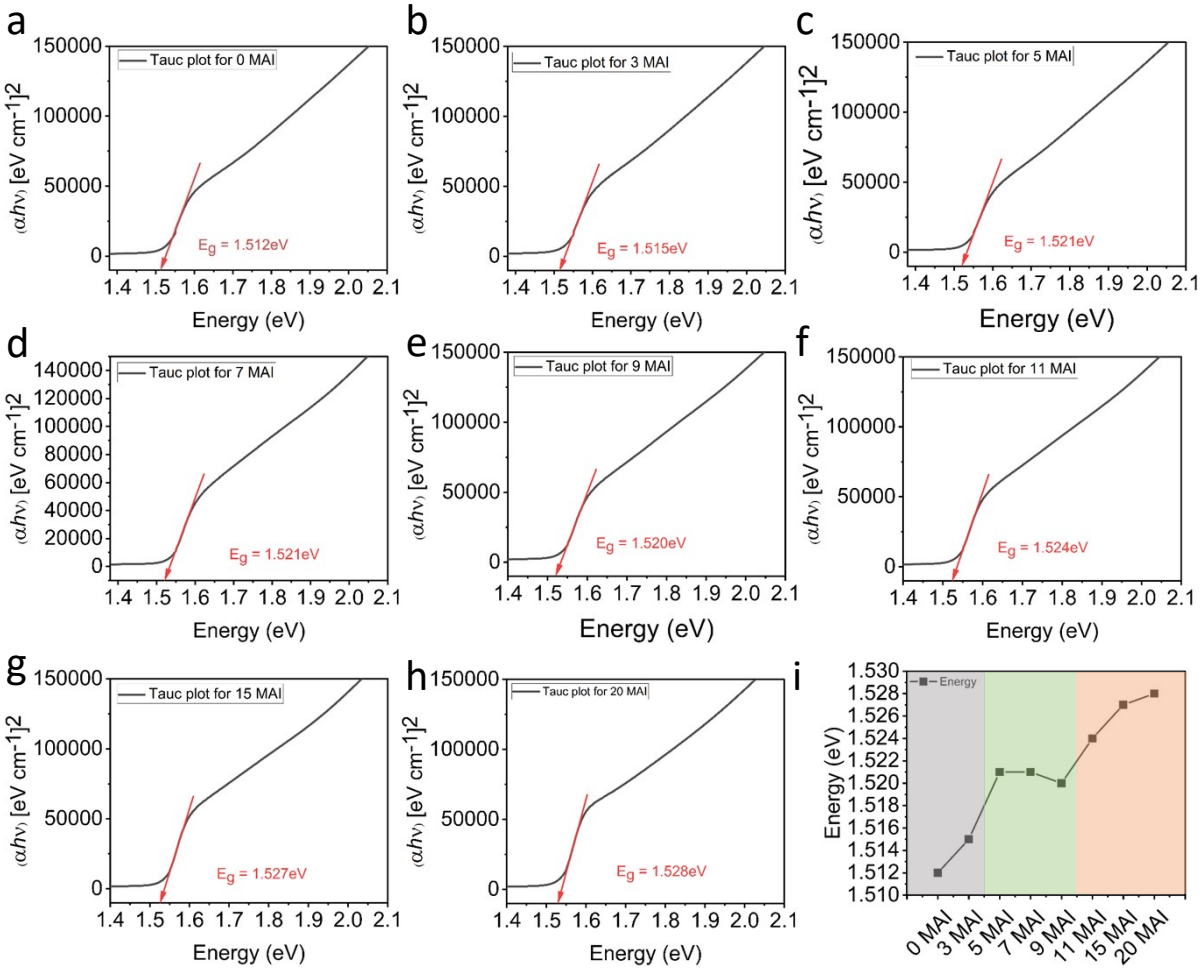

Fig. S3 Tauc-plot derived from Ultraviolet visible (UV-VIS) spectroscopy absorption coefficient data indicating energy band offset when deposited over glass substrate for the respective samples of (a) 0MAI, (b) 3MAI, (c) 5MAI, (d) 7MAI, (e) 9MAI, (f) 11MAI, (g) 15MAI, (h) 20MAI, and (i) comparing Tauc bandgap as a function of excess MAI.

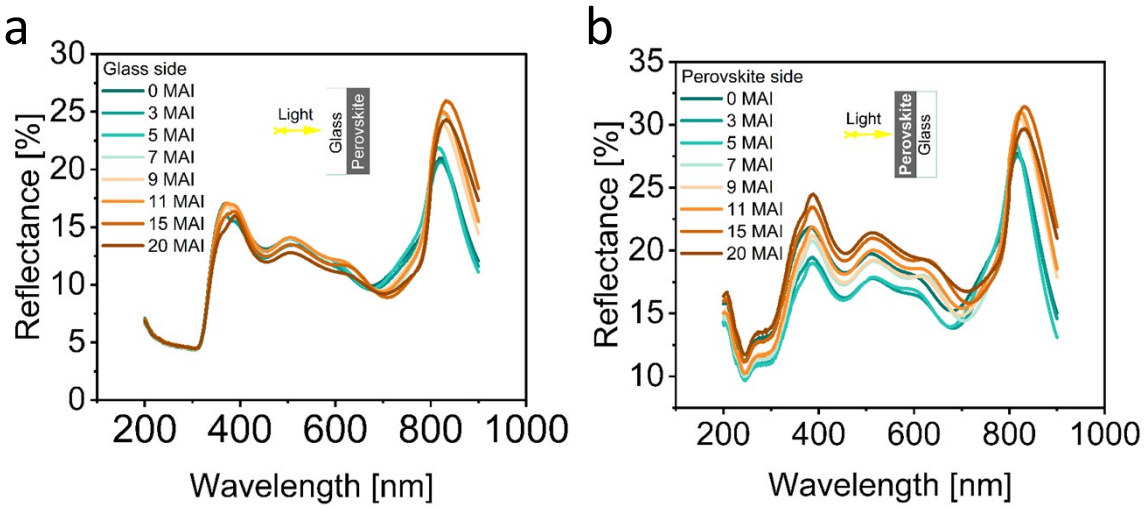

Fig. S4 Reflectance measurement of perovskite compositions with different MAI concentration measured with the help of Ultraviolet visible (UV-VIS) spectroscopy. (a) Sample illuminated from glass side, and (b) sample illuminated from perovskite side. The inset represents illumination from respective sides.

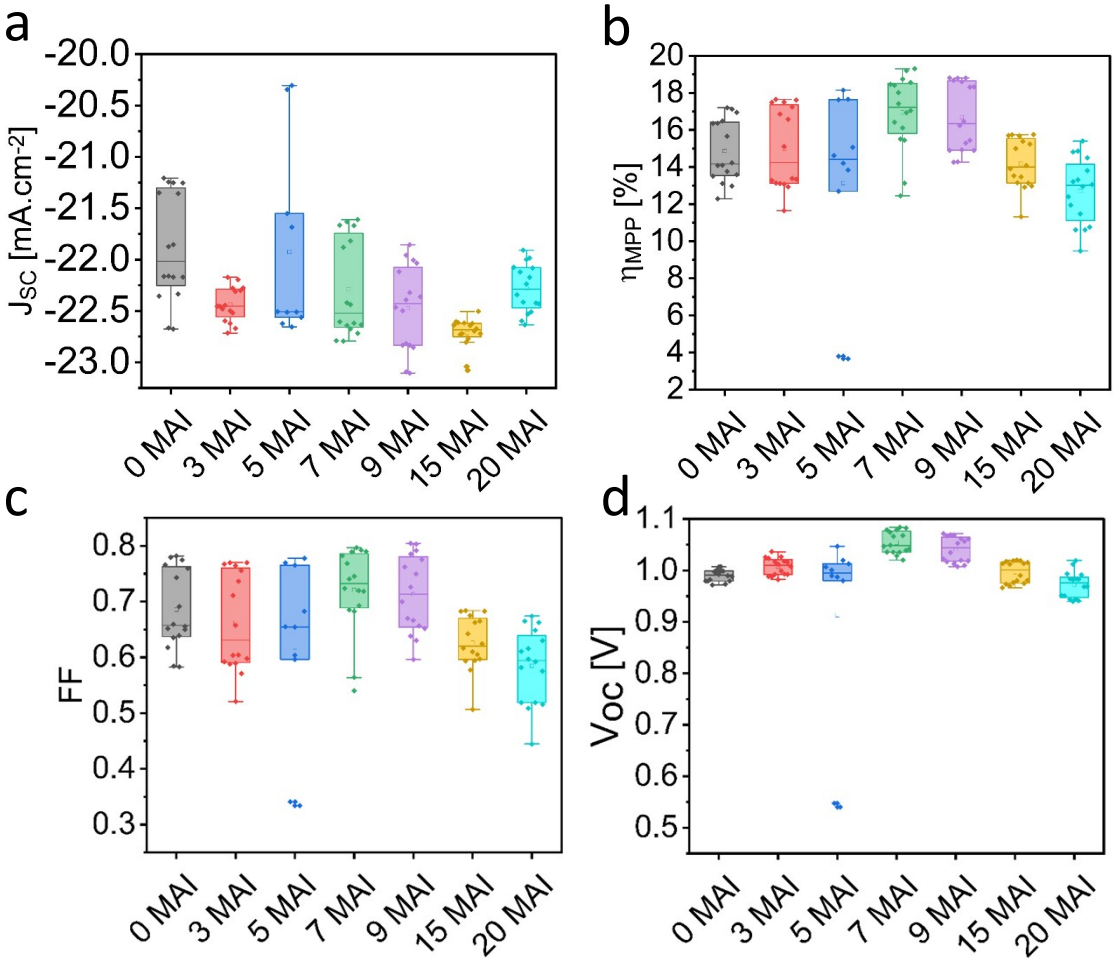

Fig. S5 Statistical results of regular n-i-p architecture device comprised of FTO/c-SnO_2/Perovskite/Spiro-OMeTAD/Au for perovskite device as a function of excess MAI content with the parameters of (a) Jsc, (b) Voc, (c) FF and (d) PCE.

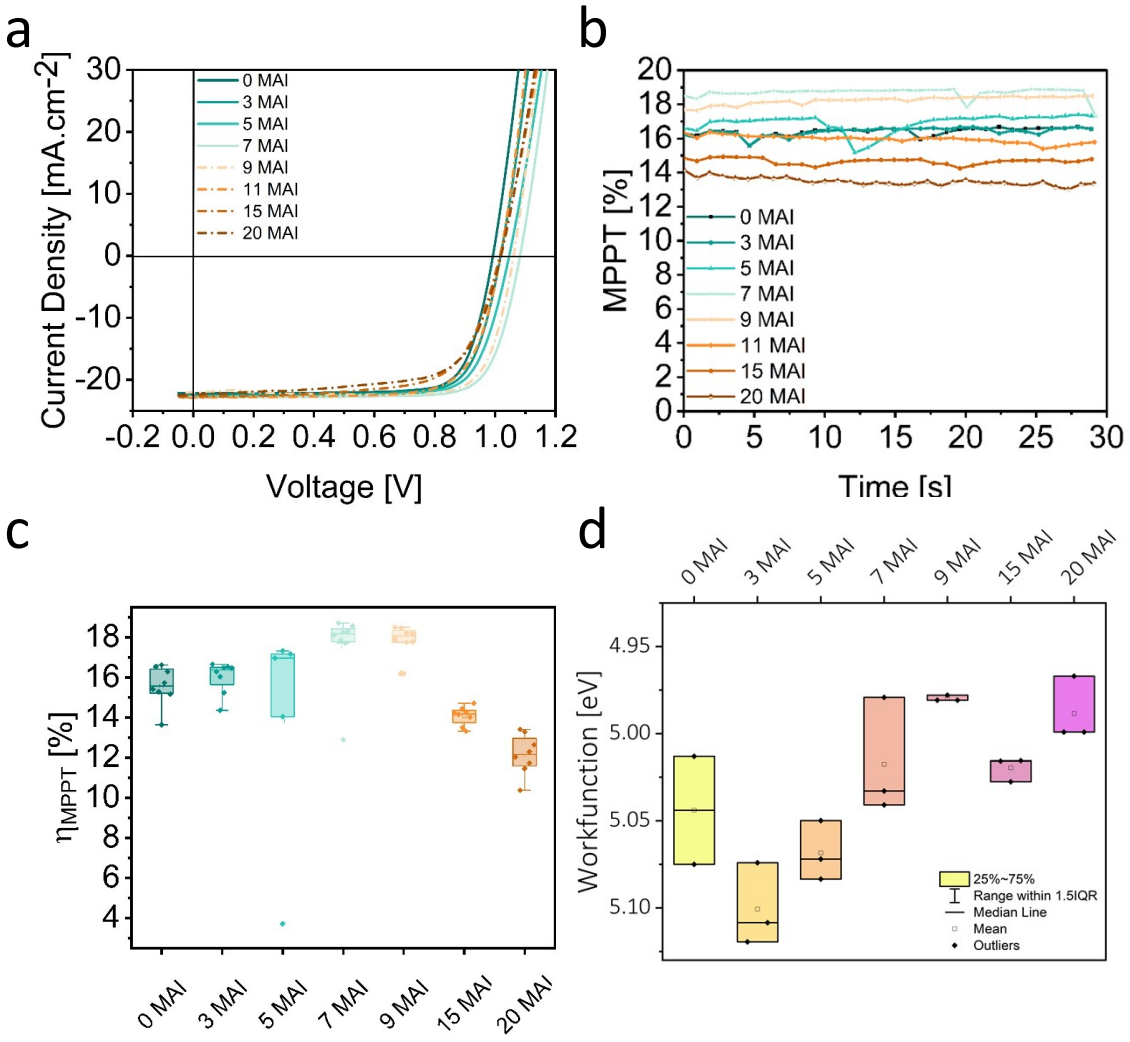

Fig. S6 Planar heterojunction regular n-i-p architecture device comprised of FTO/c-SnO_2/Perovskite/Spiro-OMeTAD/Au for perovskite device as a function of excess MAI content. (a) The current density-voltage (J-V) curve, (b) stabilized power output scanned for 30 seconds, and (c) statistical distribution of MPPT after scanned for 30 seconds. (d) Kelvin Probe measurement of various perovskite compositions as a function of MAI content. The perovskite

films were deposited on top of Indium Tin Oxide (ITO) substrates. For reference highly oriented graphene substrate (HOGS) was used and gold tip. The figure shows the statistical distribution where 3 data points were recorded for each sample.

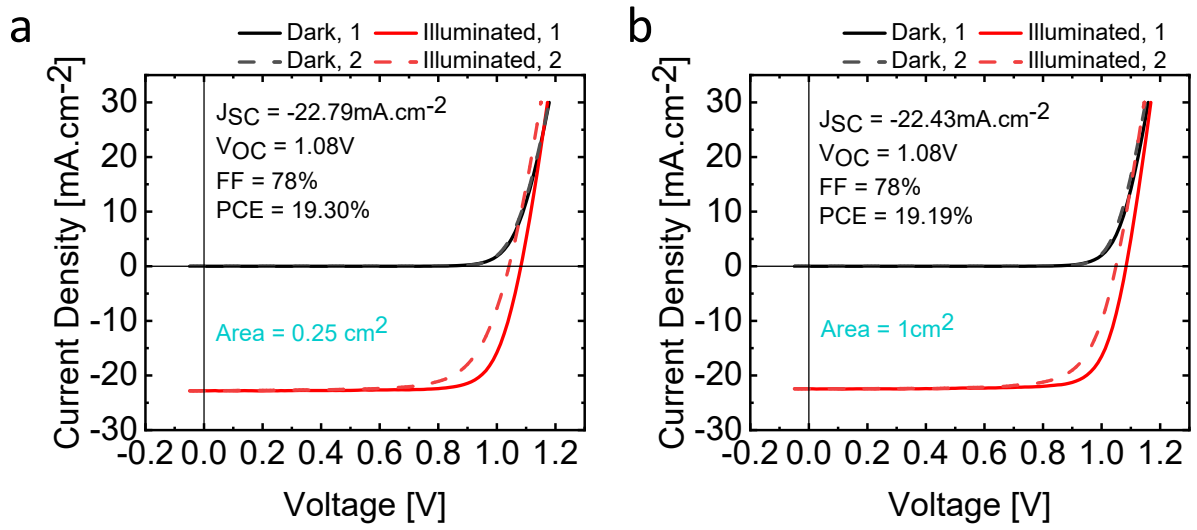

Fig. S7 The current density-voltage (J-V) curve of planar heterojunction regular n-i-p architecture device comprised of FTO/c-SnO_2/Perovskite/Spiro-OMeTAD/Au for perovskite device with 7mol% excess MAI content. The aperture area of (a) 0.25 cm^{-2} and (b) 1 cm^{-2}.

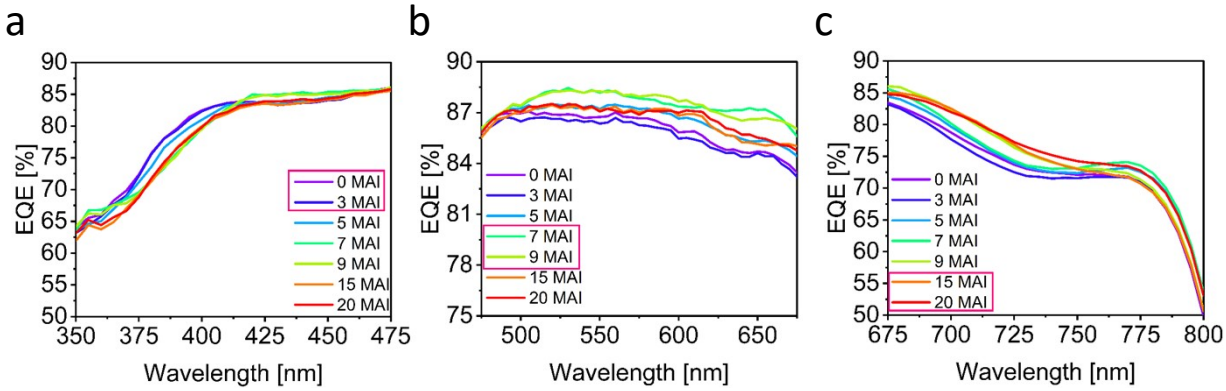

Fig. S8 External quantum efficiency spectrum of perovskite solar cells as a function of excess MAI content. (a) Respective samples in the high energy range (350-475 nm), (b) broad-range (475-67 5nm), and (c) low energy range (675-820 nm).

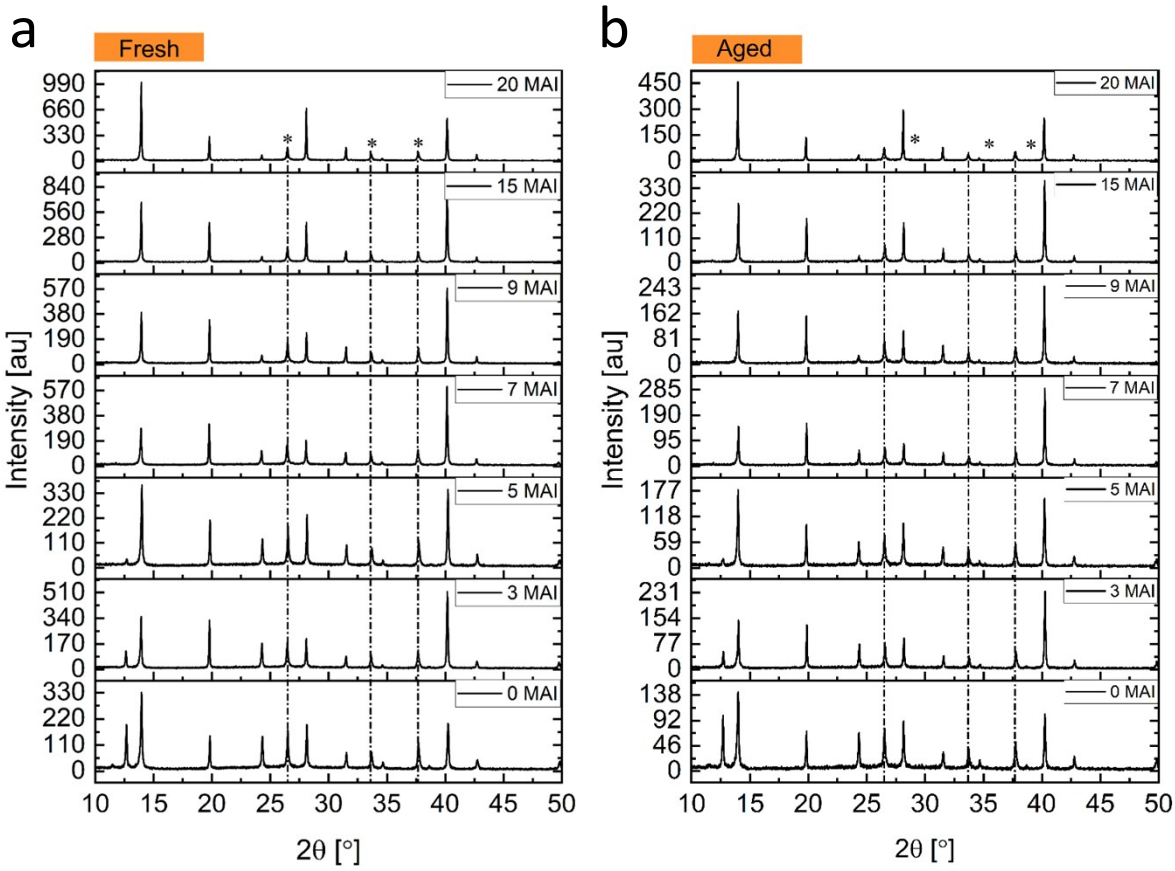

Fig. S9 The X-ray diffraction spectra of unannealed perovskite compositions with varying MAI concentrations deposited over FTO substrates. The XRD peaks corresponding to cubic phase $FAPbI_3$ (α symbol), PbI_2 (delta symbol), and FTO (asterisk symbol) are marked. (a) Fresh thin-films, and (b) 85 days aged thin-films under dark in inert.

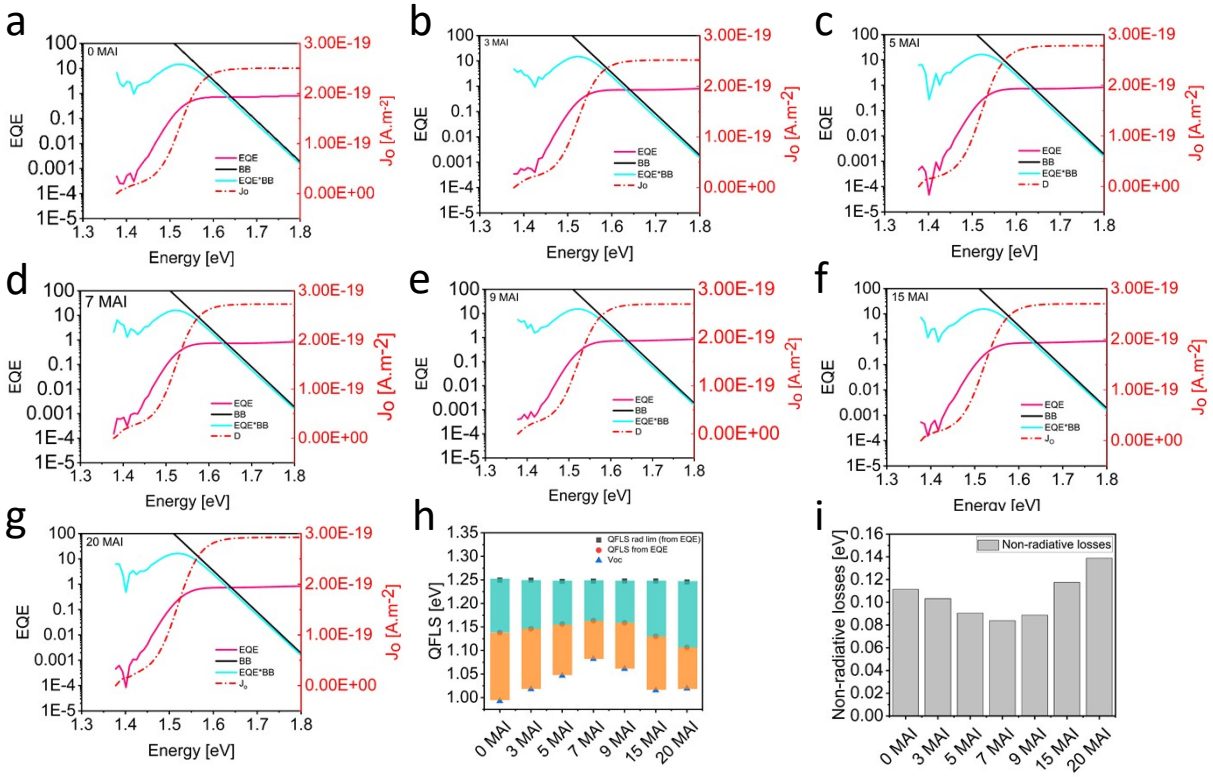

Fig. S10 The calculation of $J_{o,rad}$ (equation S2, when luminescence quantum efficiency is unity) by integrating external quantum efficiency (EQE) of our devices and blackbody spectrum ($\emptyset_{BB}$) of surrounding at 300K, as a function of excess MAI concentration. (a) 0MAI, (b) 3MAI, (c) 5MAI, (d) 7MAI, (e) 9MAI, (f) 15MAI, (g) 20MAI, (h) The black dotted line represents radiative limit for an energy bandgap of 1.53 eV and corresponding calculated QFLS (thin-film), for varying MAI concentration, and (i) Estimated non-radiative recombination losses for different MAI concentration. The low height indicates low NRR's.

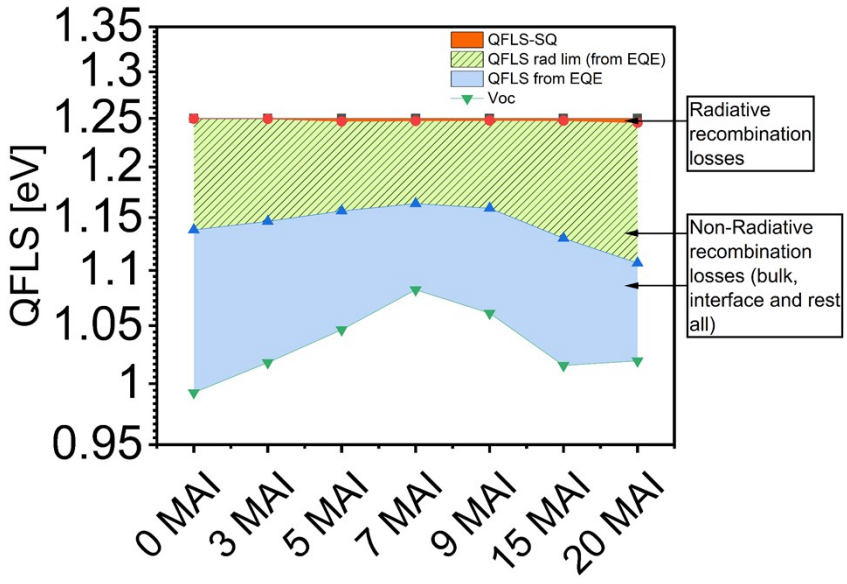

Fig. S11 The experimentally calculated quasi-fermi level splitting (QFLS) radiative-limit, $QFLS^{SQ}$ and open-circuit voltage (V_{OC}) of a solar cell is presented, as a function of excess MAI into the precursor, for a bandgap of 1.53 eV. The QFLS obtained (see supporting note 3) with the help of luminescence quantum efficiency when perovskite deposited over glass substrate. The V_{oc} of PV cell under radiative limit (V_{oc}^{rad}) is different from (V_{oc}^{SQ}) if the absorptance of PV cell deviates from a step function, which is often the case for most of practical PV technology[6]. Moreover, less steep the rise in EQE, the larger is the dark recombination current density (J_o) and the larger (V_{oc}^{rad}) is different from (V_{oc}^{SQ}). The difference in these two V_{oc} values is referred as radiative recombination losses which we highlight in orange colour[6]. The green shaded and blue region representing non-radiative losses (NRRs). The 7mol% MAI device indicating lowest losses.

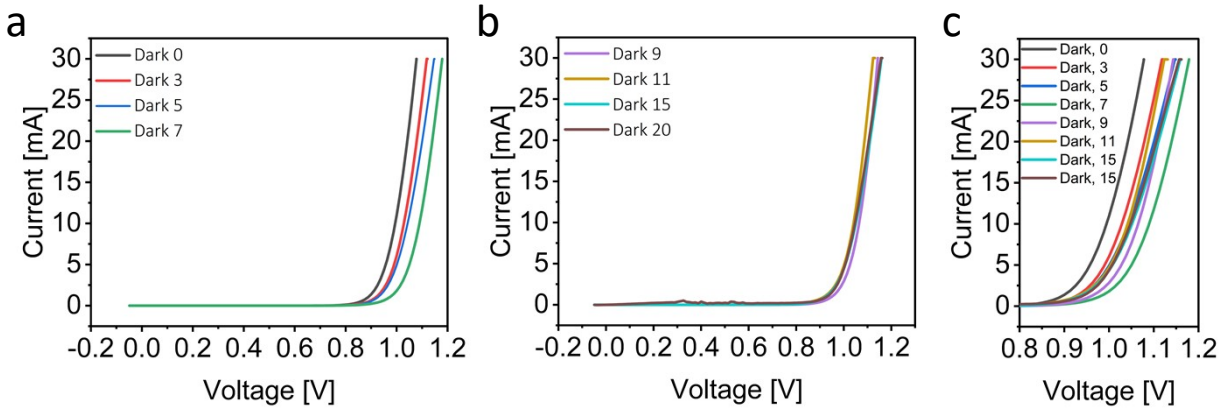

Fig. S12 The dark I-V measurement of planar n-i-p perovskite solar cells as a function of MAI concentration of (a) 0-7MAI, (b) 9-20MAI, and (c) 0-20MAI.

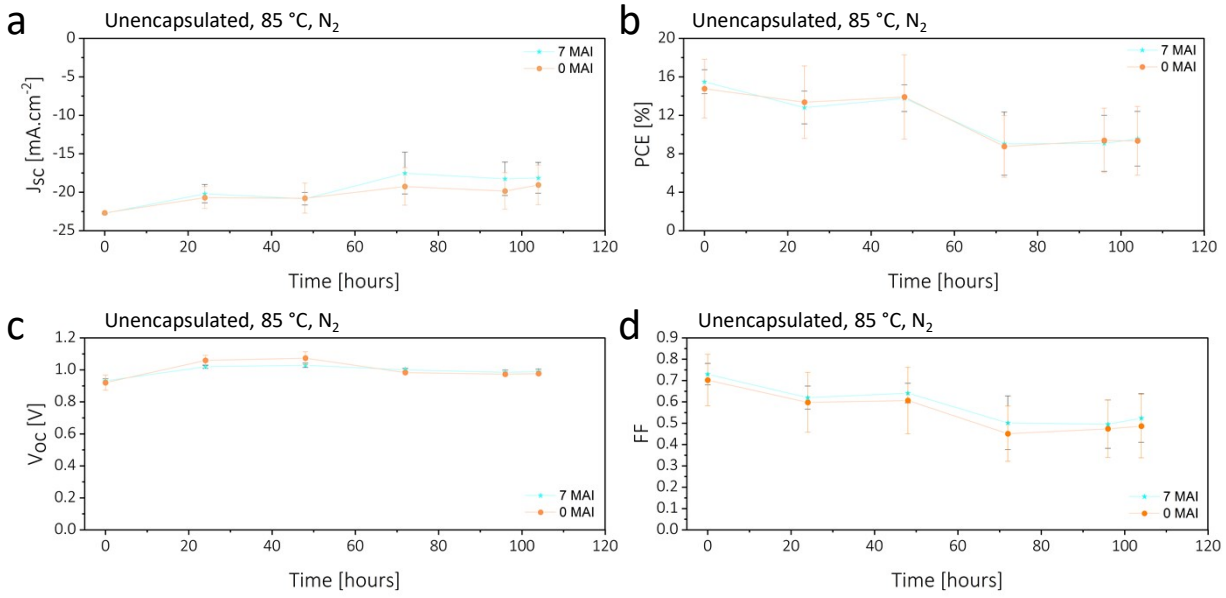

Fig. S13 Evolution of stability of regular n-i-p architecture device comprised of FTO | c-SnO_2 | Perovskite | Spiro-OMeTAD | Au samples for with (7MAI) and without MAI (0MAI) perovskite compositions. The devices were unencapsulated and kept under dark at 85°C under nitrogen. The error bars are denoted by standard deviation. (a) Current density, (b) Power conversion efficiency, (c) open-circuit voltage and, (d) fill-factor.

D. Supporting tables

Table S1 Comparison of perovskite characteristic peak position (2 theta) of (100), (110), (200), and (220) peaks as a function of excess MAI content. The parameters listed in table are extracted from X-ray diffraction spectra and corresponding calculated full width half maximum (FWHM).

Sample	(100)		(110)		(200)		(220)	
	FWHM	peak	FWHM	peak	FWHM	peak	FWHM	peak
0MAI	0.16828	13.9543	0.10592	19.82152	0.13986	28.12822	0.15812	40.24166
3MAI	0.14006	13.92234	0.09277	19.78149	0.12228	28.08681	0.13523	40.18339
5MAI	0.14913	13.97851	0.10008	19.83065	0.11597	28.14058	0.13927	40.22737
7MAI	0.15077	13.91145	0.10344	19.76003	0.11782	28.07348	0.12582	40.15473
9MAI	0.11714	13.94541	0.09273	19.78563	0.09966	28.1027	0.11483	40.17167
15MAI	0.10516	13.93896	0.08927	19.77455	0.09271	28.09237	0.11455	40.16169
20MAI	0.10049	13.93989	0.08887	19.7752	0.08754	28.09228	0.113	40.16237

Table S2 Time correlated single photon counting (TCSPC) decays measurement for perovskite samples with different perovskite composition. The samples were illuminated from the perovskite side with a 635 nm laser at a fluence of 2.41 nJ cm^{-2} represents PL lifetime of perovskite compositions as a function of excess MAI content.

Sample	Average lifetime
	s
0MAI	201.79
3MAI	218.63
5MAI	231.06
7MAI	236.18
9MAI	231.76
11MAI	229.66
15MAI	205.57
20MAI	104.32

Table S3 Photovoltaic parameters of regular n-i-p solar cells extracted for perovskite compositions with different MAI content. The devices were scanned in both reverse and forward bias direction under simulated air mass 1.5 sunlight.

	Scan direction	V_{oc} [V]		J_{sc} [mA.cm^{-2}]		FF [%]		Efficiency [%]	
		0.25cm^2	1cm^2	0.25cm^2	1cm^2	0.25cm^2	1cm^2	0.25cm^2	1cm^2
0MAI	Reverse	0.99	0.99	-22.16	-22.67	78.17	69.10	17.20	15.66
	Forward	0.97	0.98	-22.16	-22.66	63.89	58.27	13.76	12.97
3MAI	Reverse	1.01	1.02	-22.51	-22.71	76.99	71.09	17.64	16.57
	Forward	0.98	0.99	-22.45	-22.67	59.22	57.08	13.13	12.93
5MAI	Reverse	1.04	1.01	-22.65	-23.08	76.54	72	18.14	16.85
	Forward	1.01	0.96	-22.62	-23.07	60.37	57.85	13.83	12.91
7MAI	Reverse	1.08	1.08	-22.79	-22.43	78.26	78.95	19.30	19.19
	Forward	1.04	1.04	-22.79	-22.41	71.80	74.03	17.04	17.41
9MAI	Reverse	1.06	1.06	-22.03	-22.83	80.44	77.57	18.80	18.80
	Forward	1.01	1.01	-21.95	-22.85	72.61	65.63	16.23	15.29
11MAI	Reverse	1.01	1.02	-22.88	-22.97	74.04	72.52	17.24	17.10
	Forward	0.96	0.99	-22.83	-22.93	64.67	64.86	14.30	14.76
15MAI	Reverse	1.01	1.01	-22.72	-23.07	68.25	64.21	15.74	14.99
	Forward	0.98	0.97	-22.72	-23.04	62.41	50.64	13.90	11.32
20MAI	Reverse	1.01	1.01	-22.41	-22.63	67.39	64.87	15.39	14.85
	Forward	0.96	0.96	-22.34	-22.59	61.07	59.63	13.21	13.05

Table S4 The average Photovoltaic parameters of regular n-i-p solar cells extracted for perovskite compositions with different MAI content. Each data point is an average value from 8 devices for each composition. The devices were scanned in both reverse and forward bias direction under simulated air mass 1.5 sunlight.

	Scan direction	V_{oc} [V]		J_{sc} [mA.cm^{-2}]		FF [%]		Efficiency [%]	
		Average	Std. Dev.	Average	Std. Dev.	Average	Std. Dev.	Average	Std. Dev.
0MAI	Reverse	0.99	0.005	-21.88	0.54	74.42	0.045	16.27	1.01
	Forward	0.98	0.006	-21.87	0.55	62.69	0.029	13.44	0.63
3MAI	Reverse	1.02	0.007	-22.44	0.18	74.15	0.039	17.00	0.85
	Forward	0.99	0.007	-22.42	0.16	58.33	0.027	12.98	0.56
5MAI	Reverse	1.02	0.020	-22.55	0.08	77.07	0.006	17.81	0.29
	Forward	0.90	0.199	-21.91	0.98	57.57	0.136	13.83	1.03
7MAI	Reverse	1.07	0.006	-22.23	0.50	78.05	0.018	18.67	0.45
	Forward	1.03	0.008	-22.29	0.49	68.76	0.063	17.04	1.57
9MAI	Reverse	1.06	0.006	-22.50	0.39	76.73	0.045	18.34	0.78
	Forward	1.01	0.008	-22.44	0.45	65.85	0.040	16.23	0.64
11MAI	Reverse	1.02	0.019	-22.93	0.13	66.86	0.073	15.75	1.57
	Forward	0.95	0.123	-22.86	0.15	60.53	0.061	14.30	2.06
15MAI	Reverse	1.01	0.003	-22.74	0.15	66.29	0.025	15.32	0.57
	Forward	0.97	0.976	-22.69	0.15	58.92	0.036	13.90	0.77
20MAI	Reverse	0.99	0.014	-22.32	0.22	62.58	0.051	13.88	1.28
	Forward	0.95	0.011	-22.23	0.24	54.39	0.056	13.21	1.34

Table S5 Stabilized photovoltaic parameters of regular n-i-p solar cells extracted for perovskite compositions under simulated air mass 1.5 sunlight, comparing maximum power point tracking (MPPT), stabilized voltage and current density at MPPT as a function of excess MAI content.

Sample	$^{\#}\eta_{MPPT}$ [%]	$^{\#}V_{MPPT}$ [V]	$^{\#}I_{MPPT}$ [mA.cm^{-2}]
0MAI	16.61746	0.82212	-20.21289
3MAI	16.53978	0.82725	-19.99367
5MAI	17.31855	0.85827	-20.17841
7MAI	18.566	0.91989	-20.18294
9MAI	18.45632	0.88839	-20.81202
11MAI	15.60684	0.75088	-20.78461
15MAI	14.70448	0.79354	-18.53016
20MAI	13.29198	0.73003	-18.20738

* Steady state at open-circuit voltage (V_{MP}) and short-circuit (I_{MP}) condition scanned for 5seconds under 1 sun illumination

Maximum power point tracking for 30 seconds under 1 sun illumination

Table S6 Extracted integrated current density and the 1st order differentiation calculated energy bandgap from EQE band edge of perovskite solar cells as a function of excess MAI content.

Sample	integrated Jsc (mA/cm^2)	E_g [eV]
0MAI	22.5272	1.536
3MAI	22.4346	1.535
5MAI	22.7472	1.533
7MAI	22.9179	1.534
9MAI	22.9024	1.535
15MAI	22.7345	1.535
20MAI	22.8743	1.534

E. References

1 W. Shockley and H. J. Queisser, *J Appl Phys*, 1961, **32**, 510–519.

2 C. A. Bates and K. W. H. Stevens, *Reports on Progress in Physics*, 1986, **49**, 783–823.

3 L. Krückemeier, U. Rau, M. Stolterfoht and T. Kirchartz, *Adv Energy Mater*, 2020, **10**, 1902573.

4 W. Tress, N. Marinova, O. Inganäs, Mohammad. K. Nazeeruddin, S. M. Zakeeruddin and M. Graetzel, *Adv Energy Mater*, 2015, **5**, 1400812.

5 U. Rau, *Phys Rev B*, 2007, **76**, 085303.

6 P. K. Nayak, S. Mahesh, H. J. Snaith and D. Cahen, *Nat Rev Mater*, 2019, **4**, 269–285.

7 D. W. de Quilettes, S. M. Vorpahl, S. D. Stranks, H. Nagaoka, G. E. Eperon, M. E. Ziffer, H. J. Snaith and D. S. Ginger, *Science (1979)*, 2015, **348**, 683–686.

8 G. Kang, J.-S. Yoon, G.-W. Kim, K. Choi, T. Park, R.-H. Baek and J. Lim, *J Mater Chem A Mater*, 2019, **7**, 25838–25844.

9 M. Stolterfoht, M. Grischek, P. Caprioglio, C. M. Wolff, E. Gutierrez-Partida, F. Peña-Camargo, D. Rothhardt, S. Zhang, M. Raoufi, J. Wolansky, M. Abdi-Jalebi, S. D. Stranks, S. Albrecht, T. Kirchartz and D. Neher, *Advanced Materials*, 2020, **32**, 2000080.

10 P. Caprioglio, D. S. Cruz, S. Caicedo-Dávila, F. Zu, A. A. Sutanto, F. Peña-Camargo, L. Kegelmann, D. Meggiolaro, L. Gregori, C. M. Wolff, B. Stiller, L. Perdigón-Toro, H. Köbler, B. Li, E. Gutierrez-Partida, I. Lauermann, A. Abate, N. Koch, F. de Angelis, B. Rech, G. Grancini, D. Abou-Ras, M. K. Nazeeruddin, M. Stolterfoht, S. Albrecht, M. Antonietti and D. Neher, *Energy Environ Sci*, 2021, **14**, 4508–4522.